Journal of Biomechanics 88 (2019) 164–172

Contents lists available at ScienceDirect

Journal of Biomechanics

journal homepage: www.elsevier.com/locate/jbiomech
www.JBiomech.com

Development and validation of a kinematically-driven discrete element model of the patellofemoral joint ☆

Jonathan A. Gustafson [a,*], John J. Elias [b], Richard E. Debski [c], Shawn Farrokhi [d]

[a] Department of Orthopedic Surgery, Rush University Medical Center, Chicago, IL, USA
[b] Department of Research, Cleveland Clinic Akron General, Akron, OH, USA
[c] Department of Bioengineering, University of Pittsburgh, Pittsburgh, PA, USA
[d] DOD-VA Extremity Trauma and Amputation Center of Excellence, Naval Medical Center San Diego, CA, USA

ARTICLE INFO

Article history:
Accepted 26 March 2019

Keywords:
Patellofemoral
Discrete element analysis
Joint contact
Modeling
Stress

ABSTRACT

Quantifying the complex loads at the patellofemoral joint (PFJ) is vital to understanding the development of PFJ pain and osteoarthritis. Discrete element analysis (DEA) is a computationally efficient method to estimate cartilage contact stresses with potential application at the PFJ to better understand PFJ mechanics. The current study validated a DEA modeling framework driven by PFJ kinematics to predict experimentally-measured PFJ contact stress distributions. Two cadaveric knee specimens underwent quadriceps muscle [215 N] and joint compression [350 N] forces at ten discrete knee positions representing PFJ positions during early gait while measured PFJ kinematics were used to drive specimen-specific DEA models. DEA-computed contact stress and area were compared to experimentally-measured data. There was good agreement between computed and measured mean and peak stress across the specimens and positions (r = 0.63–0.85). DEA-computed mean stress was within an average of 12% (range: 1–47%) of the experimentally-measured mean stress while DEA-computed peak stress was within an average of 22% (range: 1–40%). Stress magnitudes were within the ranges measured (0.17–1.26 MPa computationally vs 0.12–1.13 MPa experimentally). DEA-computed areas overestimated measured areas (average error = 60%; range: 4–117%) with magnitudes ranging from 139 to 307 mm^2 computationally vs 74–194 mm^2 experimentally. DEA estimates of the ratio of lateral to medial patellofemoral stress distribution predicted the experimental data well (mean error = 15%) with minimal measurement bias. These results indicate that kinematically-driven DEA models can provide good estimates of relative changes in PFJ contact stress.

© 2019 Elsevier Ltd. All rights reserved.

1. Introduction

Osteoarthritis (OA) of the patellofemoral (PFJ) joint has recently gained significant attention as a major debilitating musculoskeletal disease, with studies showing incidence rates as high as 32% in individuals over the age of 50 (Hinman et al., 2014; Stefanik et al., 2013). Despite the high incidence of patellofemoral OA, the pathophysiology of this disorder remains unclear; one accepted and well-documented precursor to patellofemoral OA is patellofemoral pain (Thomas et al., 2010). Currently, one commonly accepted hypothesis for development and progression of patellofemoral pain is altered loading at the cartilage and subchondral bone levels (Powers et al., 1999; Wyndow et al., 2016). Altered PFJ loads have been found to be most directly caused by poor patella malalignment and tracking (Cahue et al., 2004; McWalter et al., 2007; Ward and Powers, 2004; Worlicek et al., 2017) that result in elevated PFJ stress (Fulkerson and Buuck, 2004; Heywood, 1961; Insall et al., 1976; Moller et al., 1989; Outerbridge, 1961).

Measuring the changes in the loading environment of the PFJ has been limited to experimental, in-vitro cadaveric tests (Ahmed et al., 1987; Haut, 1989; Huberti and Hayes, 1984; Lee et al., 1994; Lee et al., 2003). The goal of these studies was to understand the impact of altered patellofemoral alignment and tracking on patellofemoral contact mechanics. In such studies, the contact stress profile across the joint is measured to provide insight for developing improved treatments to limit pain and prevention of OA. Unfortunately, no current method exists to provide direct quantitative evidence of joint contact stress profiles in-vivo.

☆ The project described was supported by the Pittsburgh Claude D. Pepper Older Americans Independence Center through (Grant number P30 AG024827) and the National Institutes of Health (Grant number K12 HD055931).

* Corresponding author at: Rush University Medical Center, 1611 W Harrison St, Suite 204, Chicago, IL 60612, USA.
E-mail address: jonathan_a_gustafson@rush.edu (J.A. Gustafson).

https://doi.org/10.1016/j.jbiomech.2019.03.032
0021-9290/© 2019 Elsevier Ltd. All rights reserved.

To address this knowledge gap, recent advancements in numerical approximation techniques have allowed for development of elaborate subject-specific computational models to investigate the internal PFJ contact environment.

Current models of the PFJ incorporate the use of finite element (FEA) techniques (Besier et al., 2005; Besier et al., 2008; Cohen et al., 2001), discrete element (DEA) methods (Elias et al., 2004; Elias and Cosgarea, 2006; Elias et al., 2004; Elias and Cosgarea, 2007; Elias et al., 2010), or utilize a combination of subject-specific musculoskeletal computer models with accurate in-vivo experimental data (Adouni et al., 2012; Fernandez and Hunter, 2005; Schmitz and Piovesan, 2016). Validation of these prior models has been limited to replicating experimental kinematics. Considering the advancements in biplanar fluoroscopy and other in-vivo imaging methods for collecting accurate kinematic data (Bey et al., 2008), displacement-driven models of the PFJ offer significant potential to quantitatively evaluate treatment in patients long-term if these models are validated.

The primary objectives of this study were: (1) to develop a three-dimensional (3D), subject-specific modeling framework for estimating PFJ contact stress utilizing the DEA method driven by highly accurate knee joint kinematics and (2) to validate the model-estimated PFJ contact stress distribution in cadaveric knees. Model validation was carried out by comparing predicted PFJ contact stress distributions with those obtained from in vitro experiments.

2. Methods

A DEA framework was developed to employ specimen-specific kinematics to estimate PFJ contact stress. The DEA modeling pipeline is described in three parts: (1) creation of subject-specific model geometry; (2) experimental collection of kinematics and contact mechanics; and (3) DEA model simulations and validation (Fig. 1).

Two fresh-frozen (stored at −18 °C) cadaveric knees (specimen #1: Age = 52 years, Sex = Male, Weight = 81.7 kg, Height = 1.80 m; specimen #2: Age = 46 years, Sex = Male, Weight = 63.5 kg, Height = 1.75 m) were utilized for the development and validation of the modeling framework. Specimens were thawed overnight at room temperature for 24 h before testing and prepared by removing all soft tissue more than 10 cm proximal and distal to the tibiofemoral joint line except for the quadriceps tendons and capsular ligaments. Femoral and tibial ends were potted to allow for mounting of the knees in an experimental testing jig. To track the motion of the bones, registration blocks were fixed to the medial tibia, medial femur and central patellar bones using an adhesive mixture from cyanoacrylate and baking soda.

2.1. DEA model generation

To create subject-specific bone and cartilage geometry, high resolution, sagittal plane magnetic resonance images (MR) were acquired for each knee with a 3.0-T MR scanner (Siemens Medical Solutions, Malvern, PA, USA). All images were acquired using an eight-channel knee coil with a 3D, high-resolution, fat-suppressed, fast spoiled gradient recalled echo (SPGR) sequence (repetition time: 14.5 ms, echo time: 2.8 ms, flip angle: 10°, matrix: 320 × 320, field of view: 14 cm, slice thickness: 0.7 mm, pixel size: 0.44 mm, scan time of 8:58 min). This sequence has been shown to provide excellent images for distinguishing bone and articular cartilage for model development (Besier et al., 2005; Farrokhi et al., 2011). Both knees were positioned supine in an extended, unloaded position within the MR coil. To visualize the registration blocks within the MR scan, a petroleum jelly mixture was applied around the cubes prior to each scan.

Once completed, the MR images were manually segmented (Mimics®, Materialise Inc., Leuven, Belgium) to produce 3-dimensional surface models of the femur, patella, and their respective articular cartilage and registration blocks (Fig. 2). The surface

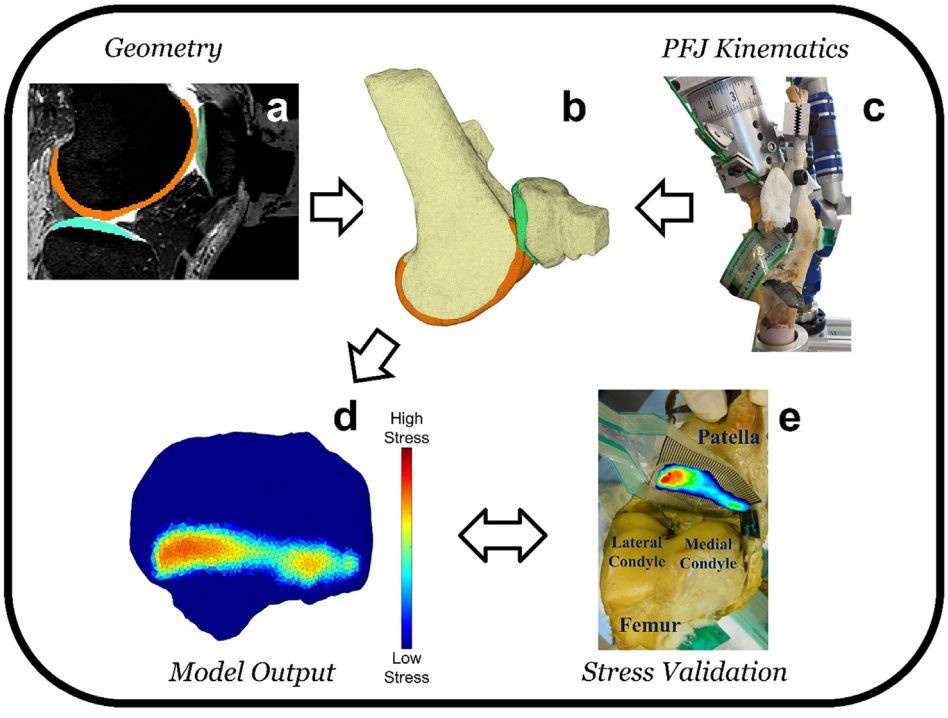

Fig. 1. Steps to create subject-specific DEA model of the patellofemoral joint driven by kinematics. Sagittal plane MR images (a) are manually segmented to create a three-dimensional surface model (b). Experimental joint kinematics (c) are collected using a mechanical digitizer and applied to the model to replicate joint positions. DEA-computed contact stress (d) is calculated and validated against experimental measures of contact stress (e).

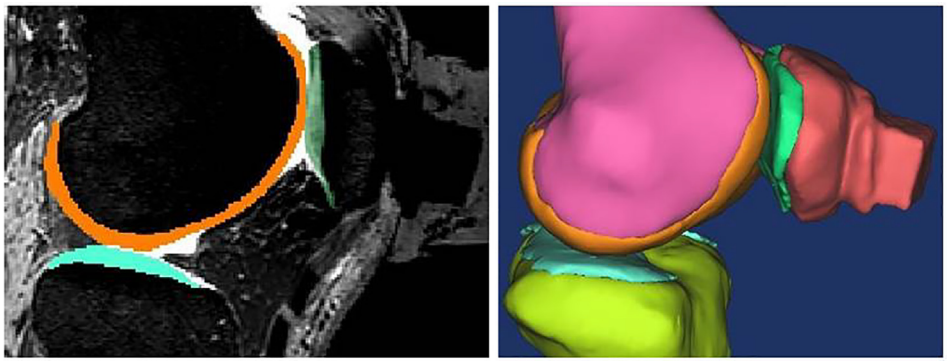

Fig. 2. Sample image of segmented masks of geometry from MRI (left) and resulting 3D model (right).

renderings were imported into an FE pre-processor (Hypermesh®, Altair Engineering Inc., Troy, MI), where a mesh refinement process was implemented. Triangular shell elements were created for both bones and articular cartilage surfaces. A mesh convergence analysis was conducted on the femoral and patellar cartilage elements through an iterative process of comparing the change in the outcome variables of interest (i.e., mean and peak contact stress) as a function of decreasing average element length. Mesh convergence was tested for the triangular shell elements with average side lengths of 4.0, 2.0, 1.0, 0.5, and 0.25 mm (Fig. 3). Results of the convergence study revealed that there were minimal changes in mean and peak contact stress between the 1 mm and 0.5 mm case (average difference of 1.4%). Therefore, an average element size of 1 mm was deemed appropriate for all computational simulations.

2.2. Testing apparatus and measuring specimen-specific kinematics

Each knee specimen was mounted in a custom designed knee testing jig that allows for unconstrained 6 degree of freedom motion throughout knee flexion-extension range with simultaneous application of tensile loads to the quadriceps tendons. Each knee specimen was positioned and loaded at two knee joint flexion angles (0° and 15° of tibiofemoral flexion) with three femoral rotation positions (neutral alignment, 5° internal, and 5° external femoral rotation) and two varus/valgus positions (5° varus and 5° valgus), for a total of 10 joint positions. These joint positions were chosen for validation as they represent clinically relevant positions during the early portion of the gait cycle, when the patella is most susceptible to peak stresses (Brechter and Powers, 2002; Perry et al., 1975). At each position, tensile loads (total force = 215 N) were applied to the quadriceps tendons [vastus medialis, vastus lateralis, and combined vastus intermedius & rectus femoris] (Pearle et al., 2007) and compressive loads (350 N) applied to the femur to simulate 50% of an individual's mean body weight (Hofer et al., 2012).

A mechanical digitizer (Faro Arm®, Lake Mary, FL) was mounted to the knee testing system and used to measure the motion of the rigid femur, patella, and tibia bone. Relative bone motions were measured by manually digitizing points on the surface of three pre-defined faces of the registration blocks attached to each bone. The digitized points were imported into custom written Matlab software (2016a, Mathworks, Natick, MA) to calculate orthonormal coordinate systems for the femur, patella and tibia bones by fitting the data points on each face to a plane equation using a least-squares optimization technique. The optimization routine generated a coordinate system for each block representing the loaded state of the knee joint at each position (Fischer et al., 2001).

2.3. DEA model positioning

To orient the unloaded computational models generated from MR scans to the loaded experimental joint positions measured experimentally, local-to-local coordinate transformation mapping—termed "coordinate registration"—was employed using coordinate systems generated for each registration block. The coordinate systems for the computational models were generated using a best-fit plane algorithm along each registration block (©2013 Geomagic Studio, 3DSystems, Rock Hill, SC). Once both unloaded and loaded coordinate systems were defined, affine

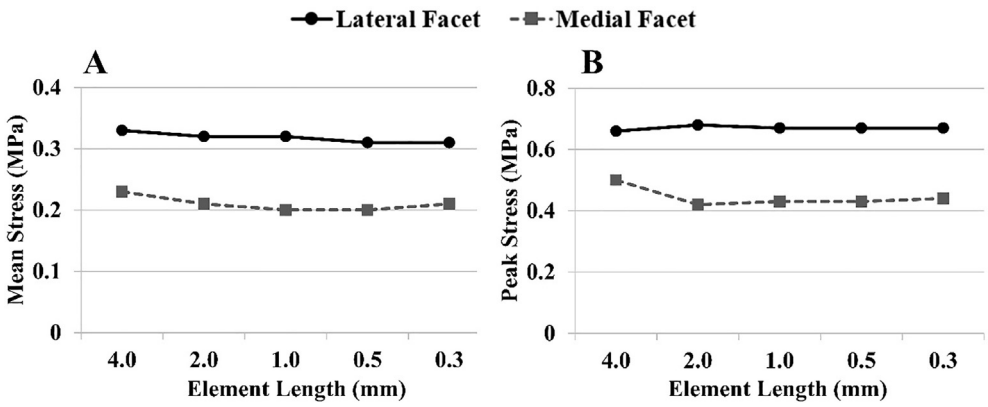

Fig. 3. Results for the mesh convergence analysis performed on the patellar cartilage elements evaluating (A) changes in mean contact stress and (B) changes in peak contact stress.

transformation matrices were formed to orient the position of the femur and patella—along with their articulating cartilage surfaces—from the MR image coordinate system to the experimental positions. This coordinate registration method has been shown to have an accuracy level of ±0.1 mm for translations and ±0.1° for rotations (Fischer et al., 2001).

2.4. Contact stress calculations and DEA simulation

PFJ contact pressures were collected at each testing position using calibrated, thin, flexible pressure sensors (K-scan Model 5051, 2.5 K psi; Tekscan Inc., South Boston, MA). Prior to testing, the sensors underwent a conditioning, equilibration, and calibration protocol (Wilson et al., 2003) using a material testing machine (Model 4502; Instron Corp., Norwood, MA). Once sensor preparation was completed, a lateral patellofemoral retinacular release was performed for each specimen to allow the pressure sensors to be inserted and secured to the *retro*-patellar surface. To characterize the spatial relationship between the pressure sensor and patellar anatomy, an outline of the sensor was recorded by pressing around the borders of the patella. This outline was then virtually registered and mapped to the patellar anatomy using measurements of the retropatellar surface recorded using a caliper (height and width).

PFJ contact stress from the DEA model was estimated using a rigid body spring method described previously (An et al., 1990; Elias et al., 2004; Genda et al., 2001; Iwasaki et al., 1998). Briefly, springs were generated in the regions of apparent cartilage overlap detected between the femoral and patellar contacting surfaces. Contact was simulated by applying the experimentally collected kinematic transformations as described above. For both DEA models, cartilage was assigned isotropic linear-elastic material properties (E = 1 MPa, v = 0.42) (Blankevoort et al., 1991). DEA contact stress was calculated using a linear elastic spring model (Blankevoort et al., 1991; Elias and Cosgarea, 2007; Kwak et al., 2000) in Matlab. The estimated contact stress was then divided into medial and lateral patellar facet regions, defined by drawing a line through the inferior apex to the superior-most point on the base of the patella. Outputs from the model included contact area and mean and peak contact stresses for each facet across the different flexion angles and rotation positions. Run time for each DEA model was less than 1 s on a desktop computer (Intel-Core i7 2.4 GHz; 32 GB RAM; 64-bit operating system).

2.5. Validation analysis

The DEA model results were validated by comparing estimates of joint contact stress distribution, mean stress and peak stress with the experimentally measured data for each knee specimen at each joint position. Additionally, comparisons were made for the lateral to medial mean and peak facet-ratio contact stress—by dividing the lateral facet mean and peak stress by those of the medial facet. The lateral to medial (LM) ratio of joint contact stress was calculated to estimate the relative change in facet-based loading across the different joint positions. The LM ratio provides a global metric of the relative distribution of the contact stress profiles. The differences in LM ratio of the contact stresses between the computational model and experimental data were used to generate Bland-Altman plots (Altman and Bland, 1983), which has been shown to be a useful tool when comparing two different measuring techniques to assess measurement bias and establish limits of agreement (LOA) of the data points. Lastly, a Pearson product-moment correlation coefficient was computed to determine the relationship between the experimental and computational area and mean and peak stress across the different knee joint positions. All statistical tests were performed in SPSS v22 (IBM, Armonk, NY).

3. Results

3.1. Contact stress

Overall, locations of contact stress were visually similar between the experimental and computational contact stress distributions for both specimens (Fig. 4). The computational model

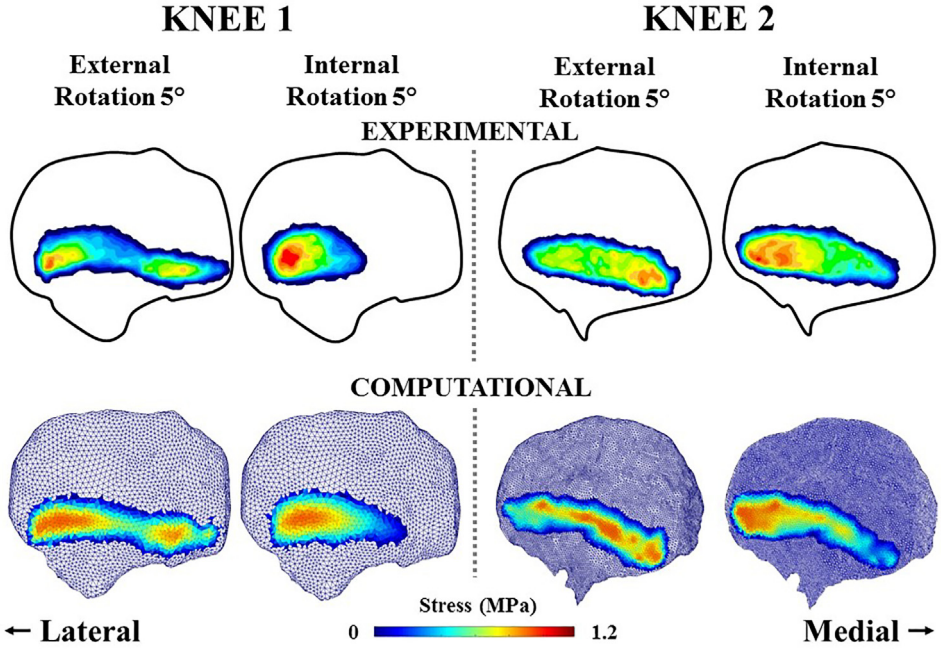

Fig. 4. The patellofemoral contact stress distribution at 15° of flexion for the experimental results (top) and computational results (bottom) for the two knees in this validation study. The stress distribution is shown for the externally rotated position and internally rotated position for each knee, demonstrating increases in lateral facet contact and stress with increasing internal femoral rotation both experimentally and computationally.

Table 1
Comparisons of contact area, mean contact stress, and peak contact stress between experimental measurements and DEA computation for both knee specimens across multiple knee flexion positions.

	Lateral Facet						Medial Facet					
Specimen #1	Contact Area (mm^2)		Mean Stress (MPa)		Peak Stress (MPa)		Contact Area (mm^2)		Mean Stress (MPa)		Peak Stress (MPa)	
Position: flexion angle, rotation angle (degrees)	Experimental	DEA	Experimental	DEA	Experimental	DEA	Experimental	DEA	Experimental	DEA	Experimental	DEA
0, external rotation 5	103	199	0.20	0.63	0.39	1.08	113	112	0.24	0.60	0.57	0.99
0, neutral	115	208	0.33	0.61	0.83	1.03	55	123	0.22	0.38	0.44	0.75
0, internal rotation 5	113	193	0.40	0.68	0.93	1.13	42	78	0.21	0.36	0.44	0.71
0, valgus 5	110	189	0.32	0.67	0.71	1.09	50	101	0.25	0.50	0.53	0.98
0, varus 5	94	174	0.29	0.6	0.71	1.02	66	66	0.23	0.48	0.53	0.91
15, external rotation 5	153	255	0.22	0.61	0.53	1.17	132	211	0.21	0.58	0.47	0.96
15, neutral	174	281	0.29	0.61	0.63	1.17	94	236	0.17	0.55	0.31	0.90
15, internal rotation 5	169	268	0.38	0.64	0.84	1.23	48	117	0.15	0.25	0.27	0.56
15, valgus 5	192	307	0.29	0.64	0.72	1.24	102	264	0.12	0.55	0.22	0.92
15, varus 5	184	294	0.30	0.63	0.66	1.19	69	242	0.14	0.51	0.27	0.84
Specimen #2												
0, external rotation 5	74	139	0.30	0.46	0.69	0.85	61	61	0.35	0.61	0.86	0.98
0, neutral	76	167	0.42	0.56	0.89	1.10	53	55	0.31	0.41	0.83	0.74
0, internal rotation 5	85	162	0.55	0.57	1.13	1.12	32	20	0.36	0.33	0.76	0.58
0, valgus 5	100	175	0.39	0.57	0.85	1.26	77	62	0.23	0.46	0.75	0.78
0, varus 5	100	162	0.38	0.52	0.86	1.03	47	53	0.24	0.36	0.73	0.69
15, external rotation 5	194	187	0.26	0.21	0.42	0.41	153	129	0.32	0.25	0.55	0.45
15, neutral	176	209	0.32	0.26	0.52	0.45	126	94	0.22	0.18	0.42	0.37
15, internal rotation 5	185	224	0.38	0.27	0.61	0.48	110	88	0.23	0.17	0.39	0.36
15, valgus 5	192	219	0.30	0.28	0.52	0.51	147	109	0.23	0.21	0.41	0.43
15, varus 5	187	234	0.33	0.30	0.57	0.55	148	102	0.23	0.21	0.41	0.42

predicted the change in stress distribution observed experimentally across the different joint positions. Both computational and experimental data determined the greatest peak stresses for the medial facet at the externally rotated positions and greatest stresses for the lateral facet at the internally rotated positions.

PFJ contact area ranged from 74 to 194 mm^2 experimentally and 139 to 307 mm^2 computationally, while patellofemoral stress ranged from 0.12 to 1.13 MPa experimentally and 0.17 to 1.26 MPa computationally for both specimens. For knee specimen #1, the computational model consistently overestimated the experimental area with a mean difference of 37% (range: 4–59%), mean stress with a mean difference of 16% (range: 1–47%), and peak stress with a mean difference of 25% (range: 7–39%) across the positions tested (Table 1). Overall, moderate, non-significant correlations were observed between the experimental and computational measures for contact area ($r = 0.47$, $p = 0.11$) and mean contact stress ($r = 0.54$, $p = 0.059$). When assessing the peak contact stress, a strong, significant correlation was found between the experimental and computational model ($r = 0.77$, $p = 0.002$).

For specimen #2, the computational model overestimated the contact area with a mean difference of 82% (range: 14–117%), mean contact stress with a mean difference of 7% (range: 1–27%), and peak contact stress with a mean difference of 19% (range: 1–40%) (Table 1). Overall, strong correlations were observed between the experimental and computational contact area ($r = 0.67$, $p = 0.03$), mean contact stress ($r = 0.84$, $p = 0.003$), and peak contact stress ($r = 0.63$, $p < 0.05$). When combining the data from both knees across all of the tested positions, a weak, non-significant correlation was found with contact area ($r = 0.27$, $p = 0.21$), while moderate-to-strong, significant correlations were found for mean contact stress ($r = 0.67$, $p < 0.01$) and peak contact stress ($r = 0.54$, $p < 0.01$).

3.2. Facet-ratio

In general, both mean and peak LM ratio of contact stress for both the DEA model and experimental data were greater than a value of 1.0, indicating greater lateral facet loading (Fig. 5). On average, the model predicted the changes in mean and peak contact stress on each facet within 15–19% of the experimental data, respectively, across the rotational positions. For specimen #1, moderate to strong correlations were observed for the LM ratio of mean contact stress ($r = 0.63$, $p = 0.02$) and peak contact stress ($r = 0.70$, $p = 0.01$) between the DEA model and experimental data. Similarly, specimen #2 showed moderate to strong correlations for the LM ratio of mean contact stress ($r = 0.85$, $p = 0.002$) and peak contact stress ($r = 0.63$, $p = 0.049$) between the DEA model and experimental data.

The results from the Bland-Altman analysis revealed low measurement bias (Fig. 6). For specimen #1, the measurement bias for the LM ratio of the mean contact stress was −0.22 (95% confidence LOA: −1.13 to 0.68). The measurement bias for the LM ratio of the peak contact stress was −0.50 (95% confidence LOA: −1.69 to 0.68). For specimen #2, the measurement bias for the LM ratio of the mean contact stress was −0.04 (95% confidence LOA: −0.38 to 0.30) and for peak contact stress was 0.14 (95% confidence LOA: −0.35 to 0.64).

4. Discussion

The objective of this study was to develop a subject-specific modeling framework employing the DEA method driven by knee joint kinematics to estimate PFJ contact mechanics. Additionally, a secondary objective was to validate this modeling framework by comparing DEA-computed contact stresses with those measured experimentally at multiple knee joint positions. The predicted stress distributions were qualitatively similar to the experimental pressure distributions, both in relative magnitude and location of contact. The DEA model also predicted the changes in joint contact stress distributions resulting from the changes in femoral rotation at the different flexion angles. A correlation analysis confirmed a moderate to strong relationship between the experimental and computational contact stress values ($r = 0.63$–0.92). Finally, a Bland-Altman analysis demonstrated a low amount of bias between the computational model and experimental data. Validation to this extent including the comprehensive outcome

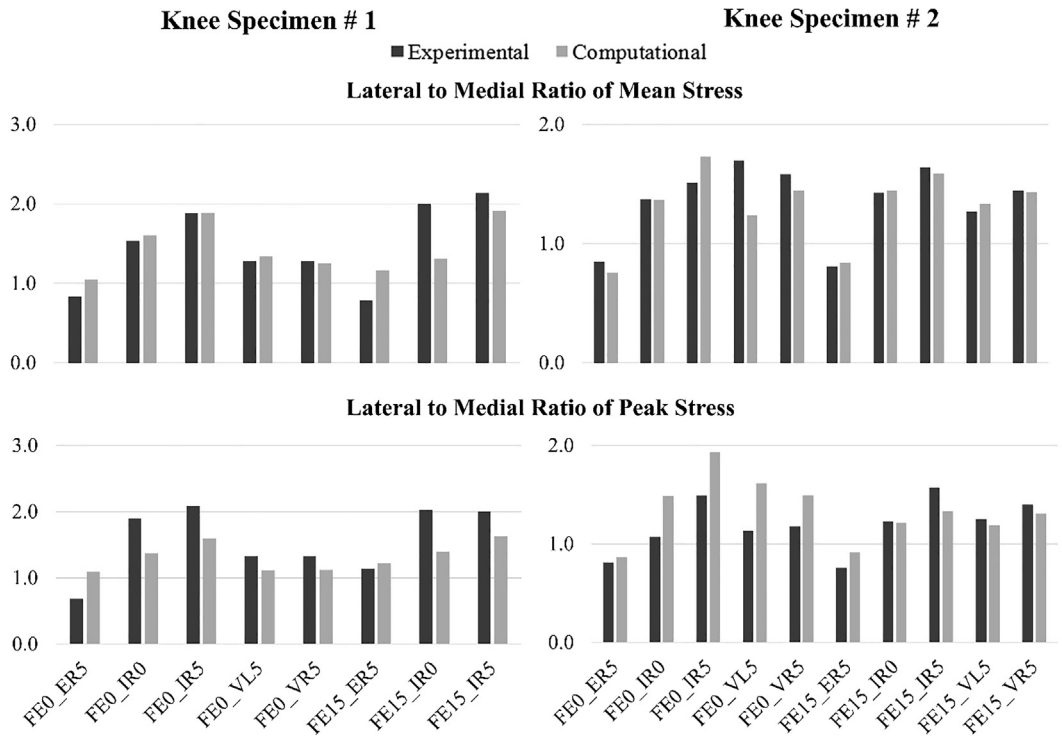

Fig. 5. Lateral to medial facet-ratio of mean (top) and peak (bottom) contact stress between DEA model and experimental data for specimen #1 (left) and specimen #2 (right) across multiple joint positions: FE = flexion angle, IR0 = neutral femoral alignment, IR5 = internal femoral rotation 5°, ER5 = external femoral rotation 5°, VL5 = valgus 5°, VR5 = varus 5°.

measures and positions tested has not been performed previously for the patellofemoral joint.

The measured experimental stresses, and subsequent computational estimates, were lower than prior studies with similar testing systems due to testing constraints for safety reasons when manually loading the knee specimens (Huberti and Hayes, 1984; Lee et al., 1994; Wilson et al., 2003). However, it is important to note that pressure-based systems, like the one used in this study, have been reported to exhibit errors in contact area over 15% and peak contact pressure estimations between 10% and 15% (Hale and Brown, 1992; Wu et al., 1998). These errors in contact pressure must be considered when using pressure sensor data as the "gold standard" for comparing model estimates of stress, which may explain some of the variability between the model and experimental data.

Direct comparison of the mean and peak stress magnitudes indicated that the model was significantly over-estimating stress—as high as 47%. However, contact stress magnitudes calculated from the model are directly related to the elastic modulus assigned to the rigid body spring model. The choice of the modulus can be tuned by the analyst to better match the magnitudes of stresses measured experimentally, if desired. For example, simply reducing the elastic modulus by 50% (0.5 MPa) for specimen #1 reduces the error in mean stress from 47% to 12% and peak stress from 46% to 18%, demonstrating the direct relationship between modulus and DEA-computed stress. We used a consistent modulus for both specimens and focused on comparing trends in stress distribution between the model and experimental data rather than predicting absolute stress magnitudes. In the current study, an elastic modulus of 1.0 MPa was chosen based on prior studies (Armstrong and Mow, 1982; Froimson et al., 1997; Krishnan et al., 2003) and does not represent the dynamic transient modulus of cartilage expected under gait loading conditions, as there were inherent experimental limitations leading to prolonged static loading (~5 to 10 min) of the specimens prior to collection of contact pressure data. Should future work look to apply this modeling technique using in-vivo data, greater elastic moduli (~3 to 7 MPa; Ateshian and Hung, 2005) would be more appropriate due to the dynamic transient properties of cartilage under gait loading conditions.

Additionally, overestimation in contact stress has been observed in prior DEA-based modeling studies (Abraham et al., 2013; Anderson et al., 2010; Elias et al., 2004; Kern, 2011) and results from the independent nature of each spring within the model such that deformation throughout the articulating surface has no effect on the neighboring springs. This is a simplification of the highly non-linear contact at the joint interface and a limitation of DEA, which cannot compute internal or depth-dependent stresses; however, this simplification can be a valuable, complimentary tool to more complex cartilage models using FEA. Furthermore, small geometrical imperfections can result in erroneous peak stress values. One method for limiting the influence of these imperfections is to compare peak stress with the 95th percentile stress data. We found a maximum difference of 9% and a 3% improvement in RMSE of peak stress when using the 95th percentile data. Considering the sensitivity of the model to moduli and potential for geometrical imperfections when predicting absolute magnitudes of stress, this study emphasized validating the relative changes in contact stress across the joint via the LM ratio.

There was good agreement between the predicted and measured changes in joint contact stress across the joint positions (<20% error). The DEA model demonstrated minimal bias (−0.16) in the LM ratio relative to the experimental data when employing a Bland-Altman analysis. The limits of agreement for the LM stress ratios in the current study ranged from −0.40 to 0.64. An important consideration of using Bland-Altman analysis is that there is no "accepted" value for validation, but rather the technique establishes limits of agreement which provide a range of values through

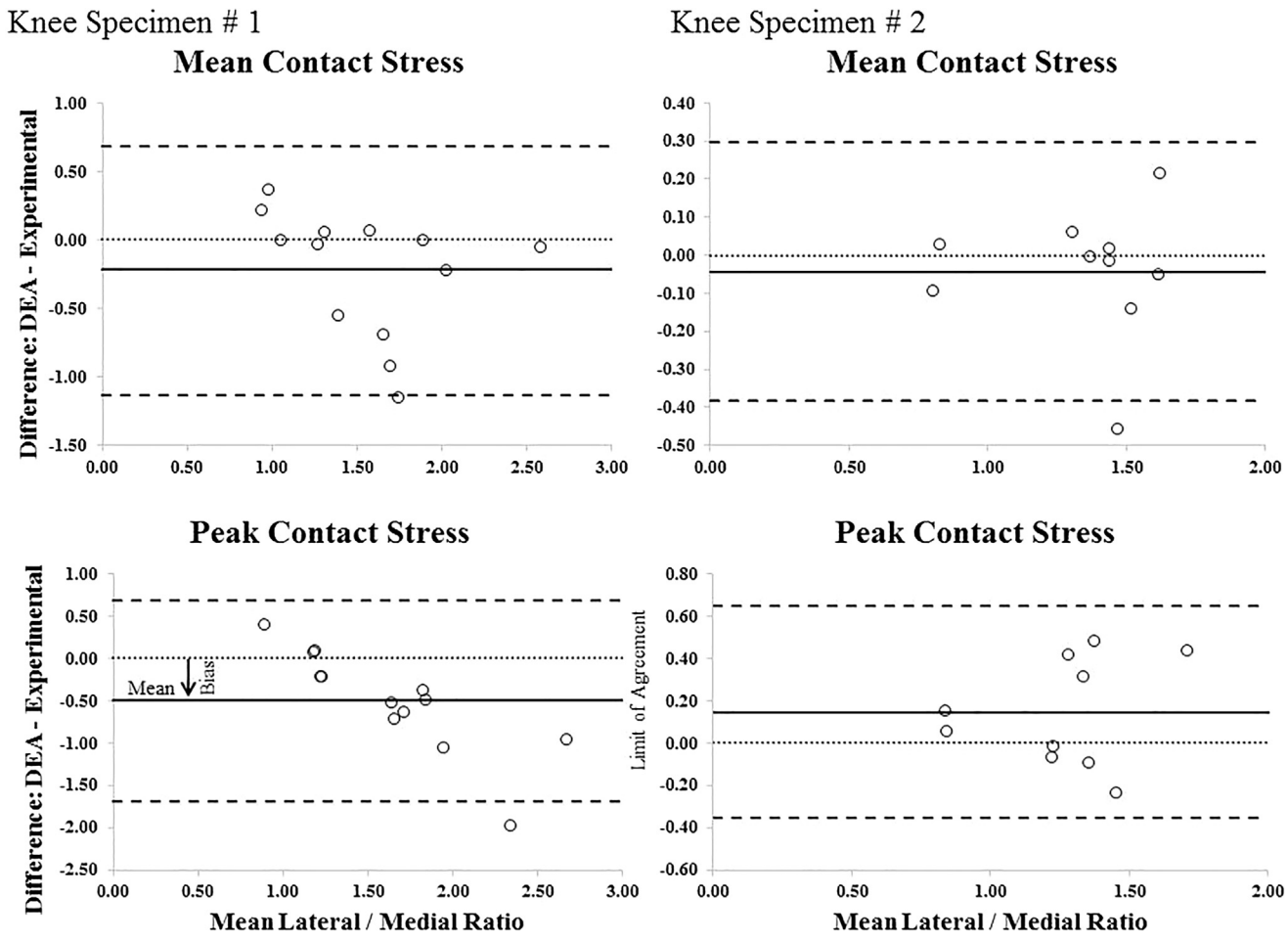

Fig. 6. Bland-Altman plots of differences between DEA and experimental measures vs. the mean of the two methods in measuring lateral to medial facet-ratio of contact stress. Plots are shown for mean contact stress (top) and peak contact stress (bottom) ratios for specimen #1 (left) and specimen #2 (right).

which the model can reliably predict experimental results (95% confidence). The DEA model predicted the changes in the LM ratio of mean and peak stress across the tested positions within 15%–19% of the experimental data, respectively. While no study to date has validated LM ratio of stresses within the PFJ, indirect estimates of LM ratio from prior force-control studies (Elias and Saranathan, 2013; Fernandez et al., 2011; Lenhart et al., 2015) show values from the current study are within a similar range (1.25–1.80). Furthermore, these prior studies used correlations as a validation metric for predicting patellar forces and stress, which does not directly assess differences between the predicted and measured data, as performed in the current study. This has important clinical implications as the current model is intended to be used in individuals with PFJ dysfunction to estimate changes in stress distribution during functional tasks. Considering the advancements in biplane fluoroscopy methods and its use for measuring changes in patellofemoral kinematics in individuals with knee OA (Bey et al., 2008; Farrokhi et al., 2015), these displacement-controlled DEA models hold promise for quantifying changes in patellofemoral stress distribution during functional tasks.

The current DEA model is dependent on the accuracy of two measurement systems: (1) the experimentally measured kinematics and (2) the image segmentation and co-registration technique. The experimental registration method used in the current study is more accurate (alignment error = ±0.1 mm) than current in-vivo imaging systems, such as biplane fluoroscopy (patella alignment error = ±0.25 mm). While the current model was developed from MR images with a 0.4 × 0.4 mm pixel size and slice thickness of 0.7 mm—deemed excellent for operating these displacement-based DEA models—the accumulated errors due to imaging, segmentation, model smoothing, and alignment must be acknowledged and have been the focus of prior work (Cohen et al., 1999; Koo et al., 2005; Thorhauer and Tashman, 2015). To summarize, image segmentation error and geometric distortion in MRI volume of the tibiofemoral joint can increase cartilage overlap by up to 0.37 ± 0.17 mm (Thorhauer and Tashman, 2015), which in part can explain the overestimates of contact area in the current study.

To understand the potential effect of MRI segmentation and kinematic errors expected from in-vivo imaging systems (i.e. biplane fluoroscopy-based systems), a sensitivity study was performed on the predicted contact mechanics. The results from this sub-analysis can be found in the Supplementary Material. In summary, increased error in estimates of cartilage overlap—up to 0.5 mm—led to a mean error in contact area of 25% (range = 16–44%) and mean error in mean contact stress of 11% (range = 8–19%). Increases in kinematic error on the order of up to ±0.5 mm or degree could alter the mean stress up to 25% and peak stress up to 24%, with a slightly lower effect on the LM ratio of 22%. These errors are substantially lower than the errors reported by Fregly et al. (>100% at ±0.5 mm) (Fregly et al., 2008), highlighting the differences between kinematic control of the patellofemoral and tibiofemoral joint. We have previously shown differences in PFJ kinematics—particularly tilt and medial-lateral translation—up to 3° and 3 mm, respectively, during downhill walking in older adults

with and without knee OA. The analysis from the current study suggests our displacement-controlled DEA modeling framework is sensitive enough to quantify the changes in mean and peak stress, as well as the relative ratio of the compartmental loading of the PFJ. However, it is important to emphasize that the current study and the estimated range of errors were only evaluated during quasi-static loading of the PFJ and should be considered prior to implementation during dynamic tasks.

In summary, the current modeling framework employed displacement driven DEA methods to estimate PFJ contact stress at multiple knee joint positions. The modeling framework was validated in terms of facet-specific contact stress distribution. These models could be used with accurate in-vivo dynamic biplane fluoroscopy techniques to estimate changes in PFJ stress distribution during functional tasks.

Acknowledgements

The project described was supported by the Pittsburgh Claude D. Pepper Older Americans Independence Center (P30 AG024827) and the National Institutes of Health (K12 HD055931). The content is solely the responsibility of the authors and the study sponsors had no role in study design, data collection, analysis, manuscript preparation, or decision making for manuscript submission.

Conflict of interest statement

The authors declare that there is no conflict of interest regarding the content of this article.

Appendix A. Supplementary material

Supplementary data to this article can be found online at https://doi.org/10.1016/j.jbiomech.2019.03.032.

References

Abraham, C.L., Maas, S.A., Weiss, J.A., Ellis, B.J., Peters, C.L., Anderson, A.E., 2013. A new discrete element analysis method for predicting hip joint contact stresses. J. Biomech. 46, 1121–1127.
Adouni, M., Shirazi-Adl, A., Shirazi, R., 2012. Computational biodynamics of human knee joint in gait: from muscle forces to cartilage stresses. J. Biomech. 45, 2149–2156.
Ahmed, A.M., Burke, D.L., Hyder, A., 1987. Force analysis of the patellar mechanism. J. Orthopaed. Res.: Off. Publ. Orthopaed. Res. Soc. 5, 69–85.
Altman, D.G., Bland, J.M., 1983. Measurement in medicine: the analysis of method comparison studies. Statistician 32, 307.
An, K.N., Himeno, S., Tsumura, H., Kawai, T., Chao, E.Y.S., 1990. Pressure distribution on articular surfaces: application to joint stability evaluation. J. Biomech. 23, 1013–1020.
Anderson, D.D., Iyer, K.S., Segal, N.A., Lynch, J.A., Brown, T.D., 2010. Implementation of discrete element analysis for subject-specific, population-wide investigations of habitual contact stress exposure. J. Appl. Biomech. 26, 215–223.
Armstrong, C.G., Mow, V.C., 1982. Variations in the intrinsic mechanical properties of human articular cartilage with age, degeneration, and water content. J. Bone Joint Surg. Am. 64, 88–94.
Ateshian, G.A., Hung, C.T., 2005. Patellofemoral joint biomechanics and tissue engineering. Clin. Orthop. Relat. Res. 436, 81–90.
Besier, T.F., Gold, G.E., Beaupre, G.S., Delp, S.L., 2005. A modeling framework to estimate patellofemoral joint cartilage stress in vivo. Med. Sci. Sports Exerc. 37, 1924–1930.
Besier, T.F., Gold, G.E., Delp, S.L., Fredericson, M., Beaupre, G.S., 2008. The influence of femoral internal and external rotation on cartilage stresses within the patellofemoral joint. J. Orthopaed. Res.: Off. Publ. Orthopaed. Res. Soc. 26, 1627–1635.
Bey, M.J., Kline, S.K., Tashman, S., Zauel, R., 2008. Accuracy of biplane x-ray imaging combined with model-based tracking for measuring in-vivo patellofemoral joint motion. J. Orthopaed. Surg. Res. 3. 38–799X-3-38.
Blankevoort, L., Kuiper, J.H., Huiskes, R., Grootenboer, H.J., 1991. Articular contact in a three-dimensional model of the knee. J. Biomech. 24, 1019–1031.
Brechter, J.H., Powers, C.M., 2002. Patellofemoral stress during walking in persons with and without patellofemoral pain. Med. Sci. Sports Exerc. 34, 1582–1593.
Cahue, S., Dunlop, D., Hayes, K., Song, J., Torres, L., Sharma, L., 2004. Varus-valgus alignment in the progression of patellofemoral osteoarthritis. Arthritis Rheum. 50, 2184–2190.
Cohen, Z.A., McCarthy, D.M., Kwak, S.D., Legrand, P., Fogarasi, F., Ciaccio, E.J., Ateshian, G.A., 1999. Knee cartilage topography, thickness, and contact areas from MRI: in-vitro calibration and in-vivo measurements. Osteoarth. Cartil. 7, 95–109.
Cohen, Z.A., Roglic, H., Grelsamer, R.P., Henry, J.H., Levine, W.N., Van Mow, C., Ateshian, G.A., 2001. Patellofemoral stresses during open and closed kinetic chain exercises. Am. J. Sports Med. 29, 480–487.
Elias, J.J., Cosgarea, A.J., 2006. Technical errors during medial patellofemoral ligament reconstruction could overload medial patellofemoral cartilage: a computational analysis. Am. J. Sports Med. 34, 1478–1485.
Elias, J.J., Mattessich, S.M., Kumagai, M., Mizuno, Y., Cosgarea, A.J., Chao, E.Y., 2004. In vitro characterization of the relationship between the Q-angle and the lateral component of the quadriceps force. 218, 63–67.
Elias, J.J., Cosgarea, A.J., 2007. Computational modeling: an alternative approach for investigating patellofemoral mechanics. Sports Med. Arthrosc. Rev. 15, 89–94.
Elias, J.J., Kilambi, S., Cosgarea, A.J., 2010. Computational assessment of the influence of vastus medialis obliquus function on patellofemoral pressures: model evaluation. J. Biomech. 43, 612–617.
Elias, J.J., Saranathan, A., 2013. Discrete element analysis for characterizing the patellofemoral pressure distribution: model evaluation. J. Biomech. Eng. 135, 081011.
Elias, J.J., Wilson, D.R., Adamson, R., Cosgarea, A.J., 2004b. Evaluation of a computational model used to predict the patellofemoral contact pressure distribution. J. Biomech. 37, 295–302.
Farrokhi, S., Keyak, J.H., Powers, C.M., 2011. Individuals with patellofemoral pain exhibit greater patellofemoral joint stress: a finite element analysis study. Osteoarth. Cartil. 19, 287–294.
Farrokhi, S., Meholic, B., Chuang, W.N., Gustafson, J.A., Fitzgerald, G.K., Tashman, S., 2015. Altered frontal and transverse plane tibiofemoral kinematics and patellofemoral malalignments during downhill gait in patients with mixed knee osteoarthritis. J. Biomech. 48, 1707–1712.
Fernandez, J.W., Hunter, P.J., 2005. An anatomically based patient-specific finite element model of patella articulation: towards a diagnostic tool. Biomech. Model. Mechanobiol. 4, 20–38.
Fernandez, J.W., Akbarshahi, M., Crossley, K.M., Shelburne, K.B., Pandy, M.G., 2011. Model predictions of increased knee joint loading in regions of thinner articular cartilage after patellar tendon adhesion. J. Orthop. Res. 29, 1168–1177.
Fischer, K.J., Manson, T.T., Pfaeffle, H.J., Tomaino, M.M., Woo, S.L., 2001. A method for measuring joint kinematics designed for accurate registration of kinematic data to models constructed from CT data. J. Biomech. 34, 377–383.
Fregly, B.J., Banks, S.A., D'Lima, D.D., Colwell, C.W., 2008. Sensitivity of knee replacement contact calculations to kinematic measurement errors. J. Orthop. Res. 26, 1173–1179.
Froimson, M.I., Ratcliffe, A., Gardner, T.R., Mow, V.C., 1997. Differences in patellofemoral joint cartilage material properties and their significance to the etiology of cartilage surface fibrillation. Osteoarth. Cartil. 5, 377–386.
Fulkerson, J.P., Buuck, D.A., 2004. Disorders of the patellofemoral joint. Lippincott Williams & Wilkins, Philadelphia.
Genda, E., Iwasaki, N., Li, G., MacWilliams, B.A., Barrance, P.J., Chao, E.Y.S., 2001. Normal hip joint contact pressure distribution in single-leg standing–effect of gender and anatomic parameters. J. Biomech. 34, 895–905.
Hale, J.E., Brown, T.D., 1992. Contact stress gradient detection limits of pressensor film. J. Biomech. Eng. 114, 352.
Haut, R.C., 1989. Contact pressures in the patellofemoral joint during impact loading on the human flexed knee. J. Orthop. Res. 7, 272–280.
Heywood, W.B., 1961. Recurrent dislocation of the patella. J. Bone Joint Surg. British 43-B, 508–517.
Hinman, R.S., Lentzos, J., Vicenzino, B., Crossley, K.M., 2014. Is patellofemoral osteoarthritis common in middle-aged people with chronic patellofemoral pain? Arthritis Care Res. 66, 1252–1257.
Hofer, J.K., Gejo, R., McGarry, M.H., Lee, T.Q., 2012. Effects of kneeling on tibiofemoral contact pressure and area in posterior cruciate-retaining and posterior cruciate-sacrificing total knee arthroplasty. J. Arthrop. 27, 620–624.
Huberti, H.H., Hayes, W.C., 1984. Patellofemoral contact pressures. The influence of q-angle and tendofemoral contact. J. Bone Joint Surg. 66, 715–724.
Insall, J., Falvo, K.A., Wise, D.W., 1976. Chondromalacia Patellae. A prospective study. J. Bone Joint Surg. 58, 1–8.
Iwasaki, N., Genda, E., Barrance, P.J., Minami, A., Kaneda, K., Chao, E.Y.S., 1998. Biomechanical analysis of limited intercarpal fusion for the treatment of Kienbock's disease: a three-dimensional theoretical study. J. Orthop. Res. 16, 256–263.
Kern, A.M., 2011. Large population evaluation of contact stress exposure in articular joints for prediction of osteoarthritis onset and progression.
Koo, S., Gold, G.E., Andriacchi, T.P., 2005. Considerations in measuring cartilage thickness using MRI: factors influencing reproducibility and accuracy. Osteoarth. Cartil. 13, 782–789.
Krishnan, R., Park, S., Eckstein, F., Ateshian, G.A., 2003. Inhomogeneous cartilage properties enhance superficial interstitial fluid support and frictional properties, but do not provide a homogeneous state of stress. J. Biomech. Eng. 125, 569–577.
Kwak, S.D., Blankevoort, L., Ateshian, G.A., 2000. A mathematical formulation for 3D quasi-static multibody models of diarthrodial joints. Comput. Methods Biomech. Biomed. Eng. 3, 41–64.

Lee, T.Q., Anzel, S.H., Bennett, K.A., Pang, D., Kim, W.C., 1994. The influence of fixed rotational deformities of the femur on the patellofemoral contact pressures in human cadaver knees. Clin. Orthop. Relat. Res. 302, 69–74.
Lee, T.Q., Morris, G., Csintalan, R.P., 2003. The influence of tibial and femoral rotation on patellofemoral contact area and pressure. J. Orthop. Sports Phys. Ther. 33, 686–693.
Lenhart, R.L., Kaiser, J., Smith, C.R., Thelen, D.G., 2015. Prediction and validation of load-dependent behavior of the tibiofemoral and patellofemoral joints during movement. Ann. Biomed. Eng. 43, 2675–2685.
McWalter, E.J., Cibere, J., MacIntyre, N.J., Nicolaou, S., Schulzer, M., Wilson, D.R., 2007. Relationship between varus-valgus alignment and patellar kinematics in individuals with knee osteoarthritis. J. Bone Joint Surg. Am. 89, 2723–2731.
Moller, B.N., Moller-Larsen, F., Frich, L.H., 1989. Chondromalacia induced by patellar subluxation in the rabbit. Acta Orthopaedica Scandinavica 60, 188–191.
Outerbridge, R.E., 1961. The etiology of chondromalacia patellae. J. Bone Joint Surg. British 43-B, 752–757.
Pearle, A.D., Solomon, D.J., Wanich, T., Moreau-Gaudry, A., Granchi, C.C., Wickiewicz, T.L., Warren, R.F., 2007. Reliability of navigated knee stability examination. Am. J. Sports Med. 35, 1315–1320.
Perry, J., Antonelli, D., Ford, W., 1975. Analysis of knee-joint forces during flexed-knee stance. J. Bone Joint Surg. 57, 961–967.
Powers, C.M., Heino, J.G., Rao, S., Perry, J., 1999. The influence of patellofemoral pain on lower limb loading during gait. Clin. Biomech. (Bristol, Avon) 14, 722–728.
Schmitz, A., Piovesan, D., 2016. Development of an open-source, discrete element knee model. IEEE Trans. Biomed. Eng. 63, 2056–2067.
Stefanik, J.J., Niu, J., Gross, K.D., Roemer, F.W., Guermazi, A., Felson, D.T., 2013. Using magnetic resonance imaging to determine the compartmental prevalence of knee joint structural damage. Osteoarth. Cartil. 21, 695–699.
Thomas, M.J., Wood, L., Selfe, J., Peat, G., 2010. Anterior knee pain in younger adults as a precursor to subsequent patellofemoral osteoarthritis: a systematic review. BMC Musculoskeletal Disord. 11. 201–2474-11-201.
Thorhauer, E., Tashman, S., 2015. Validation of a method for combining biplanar radiography and magnetic resonance imaging to estimate knee cartilage contact. Med. Eng. Phys. 37, 937–947.
Ward, S.R., Powers, C.M., 2004. The influence of patella alta on patellofemoral joint stress during normal and fast walking. Clin. Biomech. (Bristol, Avon) 19, 1040–1047.
Wilson, D.R., Apreleva, M.V., Eichler, M.J., Harrold, F.R., 2003. Accuracy and repeatability of a pressure measurement system in the patellofemoral joint. J. Biomech. 36, 1909–1915.
Worlicek, M., Moser, B., Maderbacher, G., Zentner, R., Zeman, F., Grifka, J., Keshmiri, A., 2017. The influence of varus and valgus deviation on patellar kinematics in healthy knees: an exploratory cadaver study. Knee 24, 711–717.
Wu, J.Z., Herzog, W., Epstein, M., 1998. Effects of inserting a pressensor film into articular joints on the actual contact mechanics. J. Biomech. Eng. 120, 655.
Wyndow, N., Collins, N., Vicenzino, B., Tucker, K., Crossley, K., 2016. Is there a biomechanical link between patellofemoral pain and osteoarthritis? A Narrative Review. Sports Med. (Auckland, N.Z.) 46, 1797–1808.